

MICROSTRUCTURE & CORROSION RESISTANCE FOR WC-Ti-N LAYERS DEPOSITED BY REACTIVE MAGNETRON SPUTTERING

O. A. MATEESCU^{a,b}, A. BALAN^c, Gh. MATEESCU^b, I. STAMATIN^c,
C. SAMOILA^b, D. URSUTIU^b, V. NASCOV^b

^a*AEG Progresiv SRL, Bucharest, Romania*

^b*Transilvania University of Brasov, Faculty of Materials Science & Engineering, Romania*

^c*University of Bucharest, Faculty of Physics, 3Nano-SAE Research Centre, Bucharest-Magurele, Romania*

Coatings with WC-Ti and WC-Ti-N structures have attracted interest in applications for dry lubricants working in extreme conditions. Usually, magnetron sputtering is most convenient method for coating of hard and wear-resistant structures. In this respect, WC-Ti and WC-Ti-N films are deposited in Ar/N₂ reactive atmosphere using targets WC and Ti. The topography, morphology and resistance to corrosion in aggressive environment (saline water) are related to the substrate temperature, respective the reactive atmosphere during magnetron sputtering.

(Received March 9, 2015; Accepted April 27, 2015)

Keywords: WC -Ti -N, dry lubricant, magnetron sputtering

1. Introduction

Solid lubricant coatings, unlike conventional lubricant materials, provide higher performance and durability in the tribological systems where the very low friction and wearing under extreme conditions are required (high vacuum, aerospace, high-speeds, high loads, and extreme temperatures) [1]. In such applications, the solid lubricants must accomplish multiple functions needing new design of materials, compositions and layering. Nanostructured multilayer coating or fully gradient materials are more convenient to design solid dry lubricants. There are several solid lubricants which include lamellar solids, soft metals, diamond and DLC films, lubricious oxides, very hard carbides and some polymers[2-5]. Among them, tungsten carbide (WC) is a promising material, due to its properties: high melting point, superior hardness among other carbides and nitrides, low friction coefficient, high elastic modulus, small thermal expansion coefficient, high thermal resistance [6]. In addition, it is a reliable solid lubricant with dry static friction coefficient: 0.20-0.25 for WC-WC; 0.4-0.6 for WC-Steel; 0.35 for WC-Cooper and 0.8 for WC-Iron [7]. The Vickers hardness reaches at 25-30 GPa, function of test force [8]. Unlike tungsten, WC is corrosion resistant to nearly all kinds of medium, except the mixtures of hydrofluoric acid and nitric acid at elevated temperature [9]. Other studies related to TaC, TiC and WC have shown that incorporating interstitial elements such as boron, nitrogen and carbon can improve oxidation resistance [10-15]. Interstitial elements improve only partial tribological properties such as toughness. When a combination of super-hardness (>40GPa) with high toughness and thermal stability is required, a new approach is proposed: "nanolaminate" i.e. multilayered structures made of ternary or quaternary compositions. To obtain a desired combination hardness- toughness the quaternary systems are more flexible in designing appropriate coatings. The quaternary coatings (W-C-Cr-N and W-C-Al-N) using reactive RF-magnetron sputtering (atmosphere, argon/nitrogen) and targets WC, Cr, Al revealed:

*Corresponding author: andronie@3nanosae.org

1) When the amount of tungsten was higher than 50 at% of the total metal content, a crystalline WC- phase (with partial N-substitution of C atoms) and chromium (or aluminum) nitride phases coexist in the coatings; 2) At lower tungsten content, the dominating crystalline phase is either W-doped CrN_{1-y} or AlN_{1-y} solid solution, with WC_{1-x} and small amounts of free sp^2 - bounded carbon [16]. Another study showed that W-C coatings with good corrosion resistance and capable to alleviate acid media corrosion and penetration can be synthesized by spark plasma sintering carburization method on tungsten substrate. The coated samples consist of three layers, which are a mixture of hexagonal WC and graphite, hexagonal W_2C , and body centered cubic W(C) in the sequence from the top surface to the substrate [17]. Titanium, also was taken in account in designing nanolaminates in combination with W. Titanium forms a cubic (fcc) carbide, and is more prone to form crystalline carbides than either Cr or W. Titanium addition to W-S-C coating increases the amount of crystalline carbide with significantly increased hardness with low friction properties in dry atmosphere [18,19]. W-implantation in TiN coating showed remarkably sputtering effects on the surfaces, and sharply decreased the friction coefficient and wear rate by 63.74% and 56.55% respectively [20]. Ti containing W-N coating layers are already tested for industrial applications [21]. Low nitrogen and titanium contents in W-Ti-N films lead to the best compromise between hardness and adhesion. The higher hardness values (≈ 50 GPa) were obtained for W-Ti-N films with 40–45 at.% N deposited from the W–20 wt.% Ti target in a reactive nitrogen atmosphere [22]. Ternary coatings based on Cr-W-N compositions are recently reported related to the microstructure and hardness around of 25-30 GPa [23,24].

Therefore, when employing higher carbides in combination with nitrides improve microtribological properties and resistance to corrosion. In this respect, coatings of WC-Ti and WC-Ti-N by DC-magnetron sputtering and DC- reactive magnetron sputtering in Ar/nitrogen with WC and Ti targets are investigated. The influence of magnetron sputtering deposition parameters on the topography, morphology electrical resistance and the corrosion resistance of WC-Ti /WC-Ti-N coatings on Si and stainless steel substrates are evaluated.

2. Materials and methods

2.1 Materials & sputtering parameters

Equipment. Multifunctional Sputtering Deposition system equipped with: 4 Magnetron Guns for targets with 2 inch diameter; Each of them are supplied from DC sources (600W) or from RF sources (PFG 600- RF Generator with Huettinger Automatic Match Box).

Targets and substrates: WC, Ti, stainless steel, polished Si substrates. The stainless steel substrates are for corrosion analysis and polished Si for the film characterizations by AFM.

The deposition parameters are summarized in Table 1. The pressure in the deposition chamber was set in the range 0.26-0.29Pa, bias substrate at 500V, power on the guns at 64- 67 W for WC target, respectively 6.5-8W for Ti target (exception: for sample 7 the gun power was set at 125 W for WC target and ~ 11 W for Ti target).

Table 1. Process parameters for the deposition of WC-Ti-N layers.

Sample	Sputtering target [guns]	Ar/N ₂ Flow [SCCM]	Substrate temperature [°C]	Deposition time [min]
1	WC/Ti	100/0	50	40
2	WC/Ti	100/0	550	30
3	WC/Ti	100/40	50	30
4	WC/Ti	100/40	250	30
5	WC/Ti	100/40	550	30
6	WC/Ti	100/40	250	40
7	WC/Ti	100/50	550	40

2.1 Characterization methods

AFM topography performed with SPM-NTegra Prima AFM (NT-MDT), operated in semi-contact mode, using a NSG 01 cantilever (resonance frequency: 83-230 kHz, elastic constant: 1.45- 15.1 N/m, scan rate 1Hz. The images AFM, recorded on 2.5x 2.5 μm scan surface.

The grain size distributions, surface skewness and the coefficient of kurtosis are raised from AFM topography (the histograms of the heights). Both coefficients give information related to the percentage of coverage or contacts area between two surfaces during wearing.

Sheet resistance (Ω/\square) - R_s , measured with the Four Point Probe Method, ALESSI head, W electrodes. $R_s=4.53xV/I$, where $V(V)$ is the voltage across the inside two points and $I(A)$ - the fixed current through the outside two points [25].

Corrosion resistance and the corrosion potential evaluated in an electrochemical cell by linear voltammetry. The electrochemical cell consists of three electrodes: WE=working electrode (the sample), CE=corrosion electrode (Pt) and RE=reference electrode (saturated calomel electrode). The electrolyte: saline solution, 0.1M NaCl. The corrosion tests are performed in the range -100mV- +100mV at a scan rate 1mV/s. The corrosion resistance (polarization resistance) and the corrosion potential are measured from Tafel plot. Equipment Voltalab PGstat model 301 (Radiometer Analytical)

3. Results and discussion

3.1 The influence of the substrate temperature, deposition time on the microstructure and electrical resistance

The microstructure and sheet resistance are dependent on the substrate temperature as well as on the reactive gas composition. When WC and Ti are co-sputtered on substrate in Ar plasma, there are no relevant differences in average roughness and electrical resistance (table 2, samples 1 &2).

Table 2. Specific features of WC-Ti and WC-Ti-N coatings depending on the substrate temperature and Ar/nitrogen flow ratio

Sample	Average Roughness-AFM (nm)	FWHM-AFM (nm)	Surface skewness	Coeff. kurtosis	Sheet resistance (Ω/\square)
1	0.25	0.58	0.65	4.54	22
2	0.24	0.59	-0.05	2.94	19
3	0.47	1.20	-0.12	0.74	274
4	0.34	2.14	0.490	2.46	106
5	0.23	0.57	0.12	11.33	100
6	0.74	2.05	0.268	0.137	213
7	0.75	2.14	0.130	0.115	226

The microstructures consist of small columnar grains (fig 1a,b), growing with the temperature substrate (fig 2A). The temperature substrate increases the Ti-atom mobility during deposition leading to the grain size growth/ crystallization (fig 2A, sample 1 &2). The microstructure is similar with a WC-Ti micromechanical mixture, where Ti- phase has main contribution in low electrical resistance values. The analysis of the surface morphology related to microtribological properties the grain size distribution, skewness (symmetry of the grain distribution) and the coefficient of kurtosis (how sharp is the peak and the contribution of the coarser and smaller grains), are the first

parameters to correlate experimental measurements for the friction coefficient respective, the percentage of the contact between interfaces. Samples 1 and 2 have in average a grain size distribution centered on 1.2 respective 2.7 nm (fig 2A). If both distributions are approximately symmetric (skewness coefficient in the range $-1/2 \div +1/2$) the coefficient of kurtosis decreases from 4.5 to 2.9 showing a transition from a sharp with large tails to broader one and shorter tails. On the other hand, samples 3, 4, 5 (fig 1 c,d,e) show the morphology changes when the nitrogen is introduced in the sputtering atmosphere (flow ratio $\text{Ar}/\text{N}_2=100/40$) and the substrate temperatures increase from 50 to 550°C.

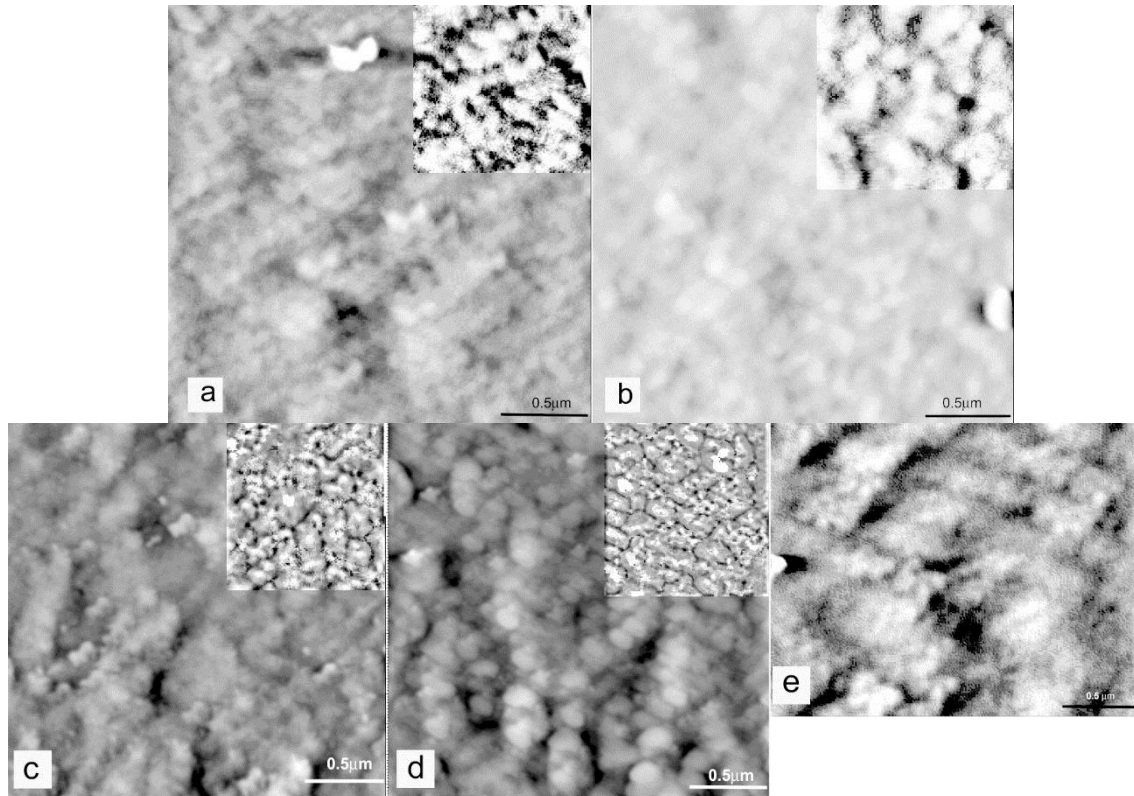


Fig. 1. AFM topography for samples 1 (a) and 2 (b) at 100 sccm flow rate of Ar working gases, substrate temperature 50°C respective, 550°C and samples 3 (c), 4 (d) and 5 (e) – for 100/40 flow rates of Ar/N₂ working gases, temperatures 50°C, 250°C, 550°C, deposition time-30min

The size distribution for samples 3,4,5 (fig 2B) shows a transition from small grains with average dimension 2.3-2.4 nm (sample 3, $t=50^\circ\text{C}$) to larger (sample 4, $t=250^\circ\text{C}$, average size 3.5 nm) and very tight (sample 5, $t=550^\circ\text{C}$, centered at 2.4 nm). If distributions are close to normal one (surface skewness is $-0.5 \sim +0.5$) the coefficient of kurtosis increases from 0.74 to 11.33, i.e. takes place a transition from no-reactive deposition to reactive deposition with complex structures W-C-Ti-N.

During deposition in reactive atmosphere: argon- nitrogen, the morphology and texture are changing from quasi-amorphous to a microstructured film consisting of small grains with local orientation. The morphology and texture are dependent of substrate temperature, as well roughness and electrical resistance (table 2, samples 3, 4, 5). In figures 1c, d, e, topographies show a transit from amorphous structure to a microcrystalline organization in well defined grains with small crystallites randomly distributed. The stacking in grains-size (fig 2B) shows an evolution from large to tight distribution centered in average at 2.2 nm (sample 5, substrate temperature, 550°C). It can be assumed that the nitrogen reactive species form very complex $\text{WC}_{1-x}\text{N}_x\text{-Ti}_{1-y}\text{N}_y$ or $\text{WC}_{1-x}\text{N}_x\text{-(TiN)}_y$ non-stoichiometric structures. The high temperature substrate increases the species mo-

bility and their reactivity, leading to a fine grain size rearrangement, in agreement with other reports [26].

The deposition time has influence on the film thickness, grain size growth, increases the electrical resistance and the roughness (table 2, samples 4, 6, 7). The average roughness increases from 0.34 nm to 0.74 nm, with the deposition time from 30 to 40 min and electrical resistance from 106 (sample 4) to 213, 226 Ω/\square (samples 6 and 7).

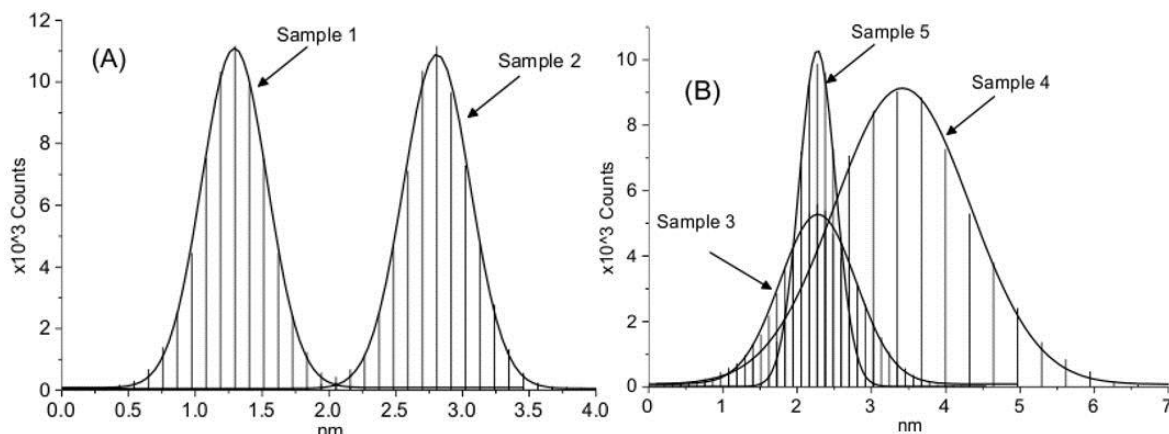


Fig. 2. Height histograms of AFM images presented in Fig. 1 of: (A) samples 1 and 2-for 100/0 flow rates of Ar/N₂ working gases and (B) samples 3, 4 and 5-for 100/40 flow rates of Ar/N₂ working gases. The continuous line represents adjustments, using the Gaussian function (deposition time 30min).

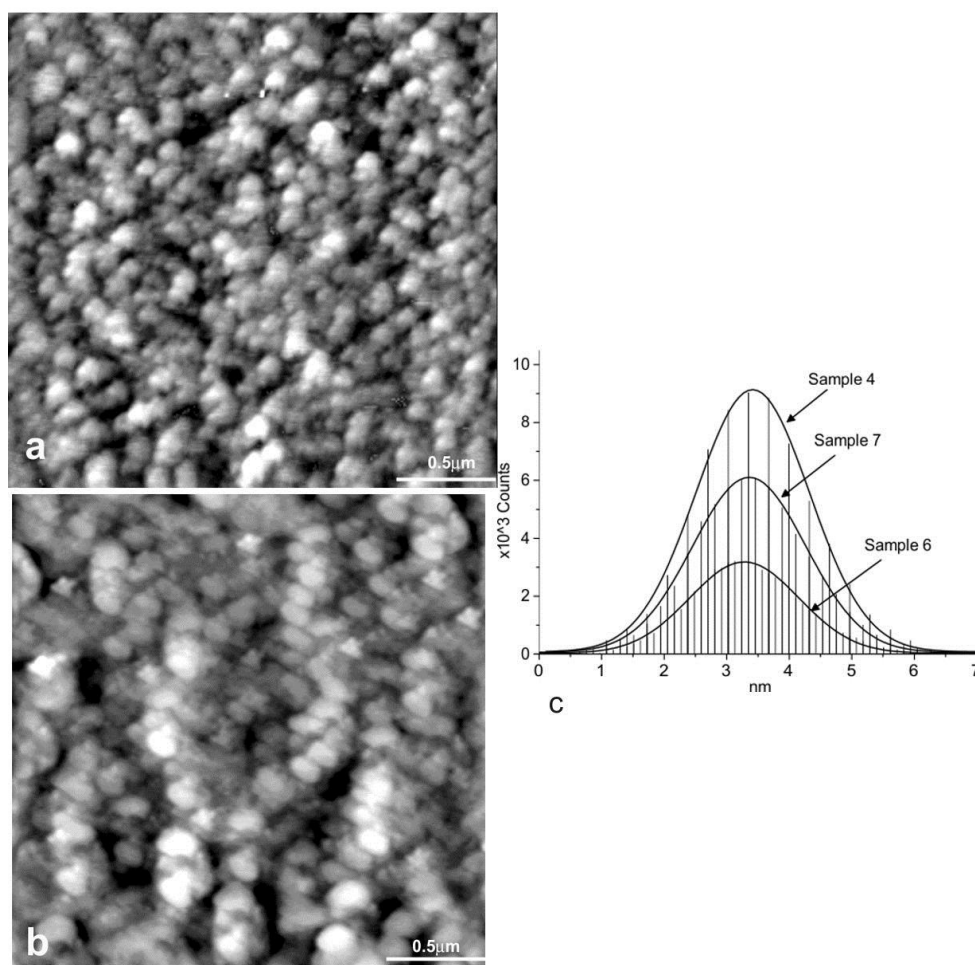


Fig. 3. AFM images of sample 6 (a) and sample 7 (b) scan surface: $2.5\mu\text{m} \times 2.5\mu\text{m}$. (c)

Height histograms for AFM images for sample 6 and 7 and comparison with 4

Samples 6 and 7 (fig 3 a,b) change the microstructure with the substrate temperature from spherulitic to small ellipsoidal grains keeping in average a size distribution centered on 3.2-3.4 nm (fig 3c). The size distribution profiles with skewness and kurtosis values close to a normal distribution with short tails show that over 250⁰C take place reactive deposition and time higher than 30 min reshape the grains consisting of new non-stoichiometric structures.

3.3 The influence of N₂ reactive gas on the corrosion resistance

The corrosion potential and the polarization resistance, determined from Tafel plot, are summarized in table 3, for representative samples, coated with WC-Ti and WC-Ti-N. The galvanic couple between substrate and coated layer is one of the most important parameter to be taken in account in designing devices with dry lubricant. The stainless steels are usually quite cathodic relative to other alloys, they exhibit electrode potentials, in saline water, from +500 to -280 mV referred to the saturated calomel electrode [27]. The electrode potential for Reference substrate, used in experiments, has -37mV, a low carbon stainless steel.

Table 3. Specific parameters of WC-Ti and WC-Ti-N coatings

Sample	Corrosion potential (mV)	Polarization resistance [kΩ]
1	-284	23
6	-66	15
7	-19	58
Ref: stainless steel	-37	81

As general rule, the coated layer should have more positive potential than stainless steel; otherwise, it loses its tribological properties. Sample 1 (WC-Ti) has a corrosion potential more negative than stainless steel which indicates WC-Ti coating has a lower corrosion resistance

The layers deposited in reactive atmosphere (Ar/N₂) have a lower negative potential increasing with the substrate temperature. The polarization resistance has the same behavior. The higher polarization resistance of the coated sample indicates that WC-Ti-N coatings are more effective in protecting against corrosion, largely.

4. Conclusions

WC-Ti and WC-Ti-N layers, deposited by standard magnetron sputtering, using N₂ as reactive gas show specific features related to the topography, morphologies, corrosion resistance. There is a critical temperature (around of 250⁰C) when the microstructures change from mechanical mixtures to complex nonstoichiometric structures. The size distribution is dependent of substrate temperature, reactive gases, deposition time. The corrosion resistance, roughness and corrosion potential are more effective for sample 7 where size distribution and microstructure is uniform and consists of hard materials with nonstoichiometric composition

“N doped WC-Ti “coated stainless steel samples exhibit much higher corrosion potentials than undoped samples, related to lower average roughness and electrical resistance.

Acknowledgements

This work was supported by a grant of the Romanian National Authority for Scientific Research, Program for research- Space Technology and Advanced Research - STAR, project number 68/2013 and PNCDI-II-46/2014

References

- [1] A. Erdemir, in: *Modern Tribology Handbook*, Vol. II, ed. B. Bhushan, CRC Press, Boca Raton, FL (2001)
- [2] C. Donnet, A. Erdemir, *Tribol. Lett.* **17**(3), 389 (2004)
- [3] N.M. Melendez, A.G. McDonald, *Surf. Coat. Tech.* **214**, 101 (2013)
- [4] L.C. Agudelo-Morimitsu, J. De La Roche, D. Escobar, R. Ospina, E. Restrepo-Parra, *Ceram. Int.* **39**, 7355 (2013)
- [5] B. Deng, Y. Tao, X. Zhu, H. Qin, *Vacuum* **99**, 216 (2014)
- [6] Y. Li, Y. Gao, B. Xiao, T. Min, Z. Fan, S. Ma, L. Xu., *J Alloys Compounds* **502**, 28 (2010)
- [7] Coefficient of Friction Reference Table-Engineer's Handbook, www.engineershandbooks.com
- [8] A. Nino, A. Tanaka, S. Sugiyama, H. Taimatsu, *Material Transactions* **51**(9), 1621 (2010).
- [9] H.O. Pierson, *Handbook of Chemical Vapor Deposition (CVD): Principles, Technology, and Applications*, Noyes Publications, LLC Norwich, New York (1999)
- [10] Z-k Chen, X. Xiong, G-d Li, Y-l Wang, *J. Mater. Sci.* **45**, 3477 (2010)
- [11] K. Vasu, M. Ghanashyam Krishna, K.A. Padmanabhan., *J. Mater. Sci.* **47**, 3522 (2011)
- [12] R. Ospina, D. Escobar, E.R. Parra, P.J. Arango, J.F. Jurado, *Appl. Surf. Sci.* **258**, 5100 (2012).
- [13] L. Yu, H. Zhao, J. Xu, *Appl. Surf. Sci.* **315**, 380 (2014)
- [14] R. Ospina, D. Escobar, E. Restrepo-Parra, P.J. Arango, J.F. Jurado, *Tribol. Int.* **62**, 124 (2013)
- [15] R. Ospina-Ospina, J.F. Jurado, J.M. Vélez, P.J. Arango, C. Salazar-Enríquez, E. Restrepo-Parra, *Surf. Coat. Tech.* **205**, 2191 (2010)
- [16] A.V. Stanishevsky, M.J. Walock, Y. Zou, L. Imhoff, A. Zairi, C. Nouveau, *Vacuum* **90**, 129 (2013)
- [17] Y. Jiang, J.F. Yang, Z. Zhuang, R. Liu, Y. Zhou, X. P. Wang, Q.F. Fang, *J. Nucl. Mater.* **433**, 449 (2013)
- [18] J. Sundberg, H. Nyberg, E. Särhammar, F. Gustavsson, T. Kubart, T. Nyberg, S. Jacobson, U. Jansson, *Surf. Coat. Tech.* **232**, 340 (2013)
- [19] H. Nyberg, J. Sundberg, E. Sarhammar, F. Gustavsson, T. Kubart, T. Nyberg, U. Jansson, S. Jacobson, *Wear* **302**, 987 (2013)
- [20] B. Tian, W. Yue, Z. Fu, Y. Gu, C. Wang, J. Liu, *Vacuum* **99**, 68 (2014)
- [21] V. Severo, L. Vilhena, P.N. Silva, J.P. Dias, D. Becker, S. Wagner, A. Cavaleiro, *J. Mater. Process. Tech.* **209**, 4662 (2009)
- [22] A Cavaleiro, B Trindade, M.T Vieira, *Surface and Coatings Technology* **174–175**, 68 (2003)
- [23] B.S. Yau, C.W. Chu, D. Lin, W. Lee, J.G. Duh, C.H. Lin, *Thin Solid Films* **516**, 1877 (2008)
- [24] Y.L. Su, C.T. Su, S.H. Yao, J.P. Yur, C.A. Hsu, T.H. Liu, *Vacuum* **80**, 1021 (2006)
- [25] M. Yamashita, M. Agu, *Jpn. J. Appl. Phys.* **23**(11), 1499 (1984)
- [26] S. Ghosh, F. Singh, D. Choudhary, D.K. Avasthi, V. Ganesan, P. Shah, A. Gupta, *Surf. Coat. Tech.* **142–144**, 1034 (2001)
- [27] F. L. LaQue, G.L. Cox, *Proc. ASTM* **40**, 670 (1940)